Asociación Argentina
de Mecánica Computacional

Mecánica Computacional Vol XXXII, págs. 3279-3294 (artículo completo)
Carlos G. García Garino, Aníbal E. Mirasso, Mario A. Storti, Miguel E. Tornello (Eds.)
Mendoza, Argentina, 19-22 Noviembre 2013

NUMERICAL IMPLEMENTATION AND PERFORMANCE OF MACROSCOPIC MODELS FOR NATURAL CONVECTION IN SQUARE CAVITIES WITH POROUS INSERTS

Cesar Venier[b], Enzo Dari[a] and Federico Teruel[a]

[a]*Division de Mecanica Computacional - Centro Atomico Bariloche*
Instituto Balseiro-UNCuyo-CNEA, Av. Bustillo Km 9.5 S8400GLN Bariloche, Argentina

[b]*Centro Internacional de Metodos Computacionales en Ingenieria (CIMEC)*
INTEC-UNL-CONICET, Guemes 3450 S3000GLN Santa Fe, Argentina

Keywords: CFD, Porous Media, Natural Convection, Darcy Model

Abstract. The study of problems dominated by natural convection through obstacles is of relevance in various fields of engineering. We may find examples where obstacles can be modeled explicitly (i.e. heat exchangers) and examples where it is convenient and practical to avoid this representation considering the obstacles as a porous medium (i.e. the cooling tank of an electrical power transformer). In this work, two-dimensional numerical solutions are presented for a variant of the classical problem of natural convection in a square cavity with Dirichlet boundary conditions. The cavity has been divided into two regions. In one region, the flow circulates in a clear space, while in the other one, the flow circulates through an array of circular solid obstacles. This can be simulated employing the actual geometry (direct simulation) or with a porous media model. In the last one, the region with obstacles is replaced by a homogeneous region where the conservation laws are affected by the interaction between the fluid and solid faces, and this interaction is represented by characteristics parameters of the medium, like the porosity and the permeability. A FEM-based program has been used to carry out the simulations. We have been able to verify the good performance of the porous model against the direct simulation in the laminar regime in terms of the velocity and temperature profiles, stratification levels and heat transfer through the vertical wall of the cavity. The main advantage in the use of porous models is the significant reduction in the computational cost. In this work we have been able to carry out porous model simulations in a third of the total time consumed by the direct simulation of the problem with the same amount of computational resources.

1 INTRODUCTION

In a porous medium, the solid-liquid interface morphology may be very complex. This is straightly related with the large computational costs involved to solve the boundary layer in solid-liquid interface. One of the main advantages in the development of a macroscopic porous media model is to lower the computational costs required to carry out numerical simulations. Additionally, there are numerous examples were the cost to map the solid-liquid interface is excessive and the use of macroscopic models becomes the best approach. These aspects motivate the development of porous models.

According to Kaviany (1995), the first steps in the development of porous media models may be attributed to the work of Darcy. The theory of Darcy, based on experimental results, states that the pressure gradient in a forced flow through an obstructed medium is linearly related to the velocity. Later on, other researchers (**?**Brinkman, 1947; Ergun, 1952) came up with extensions of the Darcy law to account for flows under different conditions than those considered by Darcy (e.g. large Reynolds numbers).

These porous media models were defined by a new set of conservation equations developed by the contributions of Slattery (1969), Whitaker (1969, 1996) and Hassanizadeh and Gray (1979a,b). The use of volumetric average theory applied to the Navier-Stokes equations allowed to develop a model that seeks to represent the dynamics of incompressible fluids through porous media at a macroscopic level (i.e. at a length scale much larger than the scale of the pore and much lower that the scale of the system). Using the same approach, Carbonell and Whitaker (1984) came up with a model for the thermal diffusivity due to the presence of solid obstacles.

In particular, porous models have also been developed for natural convection problems. Natural convection phenomena through porous media can be found in many engineering applications. Residual treatment, oil extraction, power transformers cooling systems, nuclear reactors and many kinds of heat exchangers are examples of the problems that motivate the present work. Recent implementations of macroscopic equations on natural convection problems may be found in the works of Massarotti et al. (2003), Braga and de Lemos M.J. (2005) and Merrikh and Lage (2005). These researchers carried out numerical simulations of natural convection through solid obstacles arrays in a square cavity for different Rayleigh numbers. In these cases, the mean Nusselt number computed employing porous models, shows good agreement with that obtained from direct simulations.

The motivation of this work is to implement a solver for the porous media model and to carry out a detailed comparison of flow variables obtained from both porous and direct models. Two approaches are therefore carried out. The first one is based on the two-dimensional simulation of a natural convection problem in a square cavity which consists in two regions, one where the fluid flows freely and other where the fluid flows through an array of solid circular obstacles. In the second approach, a porous model is implemented in the obstacles region to avoid the explicit representation of the solid-fluid interface. The first approach is usually referred as an heterogeneous model, continuum model or a microscopic model, while the second approach is usually referred as an homogeneous model, porous-continuum model or a macroscopic model. In this work we will identify this approaches as microscopic and macroscopic models respectively. With the numerical solution of both approaches, the differences between the velocity and temperature fields will be employed to evaluate the accuracy of the macroscopic model on a quality level, while, in a quantity level, the local and mean heat transfer on a vertical wall will be compared.

In the next section, we present the partial differential equations that model our problem,

the geometry of our domain, the boundary conditions and the mesh adopted for each model. We briefly discuss some concepts of the numerical method that has been applied to solve the macroscopic model. Later on, we discuss the selection of the macroscopic parameters for this problem. Finally, we present results of velocity and temperature fields and heat transfer through a vertical wall with both models for Ra $= 10^8$, 10^9 and 10^{10}.

2 MODELING DESCRIPTION

2.1 Computational domain

In this work we are interested in studying the behavior of a porous media model in natural convection regime considering cases that appear in real applications. Therefore, we propose a problem with the characteristics of real cases in terms of boundary conditions, fluid properties and global dimensions. In Figure 1, we present the domain geometry for the microscopic model of the problem, which consists of a square cavity of 1.05 m $\times$ 1.05 m and an "in-line" array of 49 circular obstacles of 28.2 mm of diameter. If the reader imagines a virtual subdivision of our domain in 9 squares of 0.35 m, the obstacles array would be located in the right-central quadrant. There is also a buffer wall that restrict the inlet-outlet lateral flow to the obstructed region. The domain geometry for the macroscopic model is equivalent to the first one, with a porous homogeneous medium replacing the region with solid obstacles.

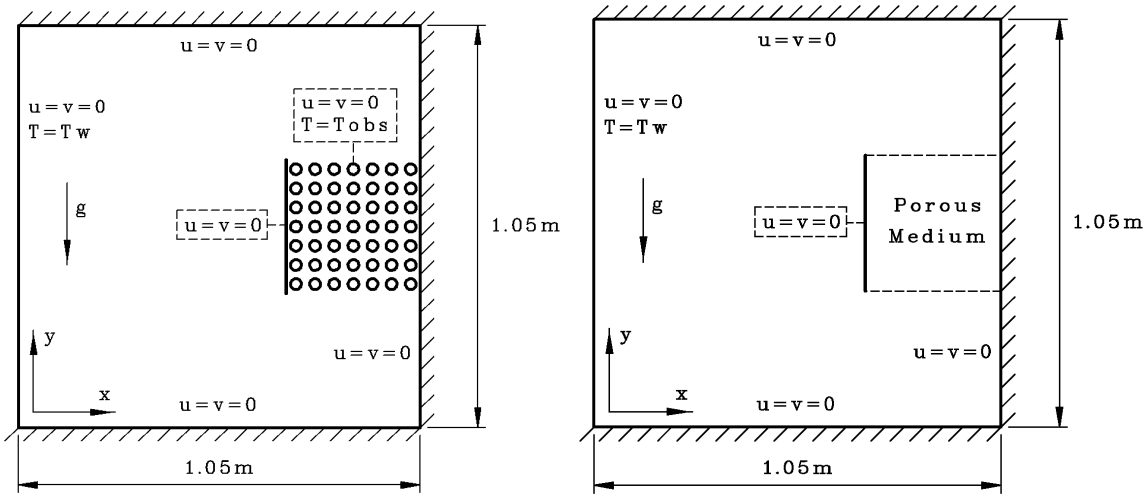

Figure 1: Schematic of the microscopic (left) and macroscopic (right) model case

For the microscopic model we use an unstructured grid of 106111 triangular elements and 54769 nodes, while for the macroscopic model we use a grid of 74285 triangular elements and 37763 nodes.

2.2 Governing equations

The differential equations that model the behavior of incompressible flows through porous media are:

$$\begin{cases} \nabla\cdot\overline{\mathbf{u}} = 0 \\ \\ \dfrac{\partial\overline{\mathbf{u}}}{\partial t} + \nabla\cdot\left(\dfrac{1}{\phi}\,\overline{\mathbf{u}}\,\overline{\mathbf{u}}\right) = -\phi\,\nabla\overline{p}_l + Pr\,\nabla^2\overline{\mathbf{u}} + Ra\,Pr\,\overline{T}_l - \dfrac{Pr}{Da}\,\overline{\mathbf{u}} \\ \\ \dfrac{\partial\overline{T}_l}{\partial t} + \overline{\mathbf{u}}_l\cdot\nabla\overline{T}_l = \nabla\cdot\left(R_k\,\nabla\overline{T}_l\right) + R_h\,(1-\overline{T}_l) \end{cases} \tag{1}$$

In (1), the variables are presented in a dimensionless form. We define our dimensioned variables (ψ^*) as:

$$x^* = Lx,\; u^* = \frac{\alpha}{L}u,\; t^* = \frac{L^2}{\alpha}t,\; p^* = \frac{\rho_0\alpha^2}{L^2}p,\; T^* = T_0 + T\Delta T$$

$$Pr = \frac{\nu}{\alpha},\; Ra = \frac{g\beta\Delta T L^3}{\nu\alpha},\; Da = \frac{K}{L^2},\; R_k = \frac{k_e}{\phi k},\; R_h = \frac{HA_{LS}L^2}{\phi k dV} \tag{2}$$

And the closure is given by the Boussinesq approximation:

$$\rho^* = \rho_0^*\left[1 - \beta\,(T^* - T_0^*)\right] \tag{3}$$

It is important to mention that the Darcy model (given by the addition of the last term in the momentum equation of the system (1)) may not be the proper way to model a flow restriction in natural convection problems. We will employ this model but this issue will be discussed further on.

The boundary conditions of the microscopic model are no-slip and no-penetration at the cavity walls and obstacles, and adiabatic conditions in all boundaries except the left vertical wall and the obstacles for which Dirichlet conditions, denoted by T_w and T_{obs} respectively, are applied. For the macroscopic model, the boundary conditions will be the same of those described for the microscopic model, except for the region with obstacles, in which a heat source will be considered.

These homogeneous equations may be reduced to the classic Navier-Stokes-Boussinesq equations for $\phi = 1$, $Da \to \infty$, $R_k = 1$ and $R_h = 0$. This means that we can use the same algorithm to solve the macroscopic problem at both the porous and the free region, as well as for the microscopic model.

2.3 Numerical method

If we try to solve the discretized Navier-Stokes and energy equations using the standard Galerkin finite element method, two numerical issues may arise. The first one is due to the Babuska-Brezzi condition (Babuska, 1971; Brezzi, 1974) which states that the velocity and pressure field has to have different interpolation order. The second one shows when we have an advection-dominated problem in which we may have oscillating solutions near boundary walls. The same behavior could be found if we have a low Darcy number. In this work we use a stabilized finite element method solver, developed in the PAR-GPFEP plataform (Buscaglia,

1995), to overcome this numerical instabilities. The interested reader may refer to the work of Codina and Blasco (2000) to a detailed explanation on the stabilization for incompressible Navier-Stokes equations. The temporal discretization was made with the Theta method and the algorithm scheme may be formulated as:

$$\begin{cases} \nabla\cdot\overline{\mathbf{u}}^{n+1} = 0 \\ \\ \dfrac{\overline{\mathbf{u}}^{n+1}-\overline{\mathbf{u}}^{n}}{\Delta t} + \dfrac{\overline{\mathbf{u}}^{\gamma}}{\phi}\cdot\nabla\overline{\mathbf{u}}^{n+\theta_1} = \\ -\phi\,\nabla\overline{p}_l^{n+1} + Pr\,\nabla^2\overline{\mathbf{u}}^{n+\theta_1} - \dfrac{Pr}{Da}\,\overline{\mathbf{u}}^{n+\theta_1} + \dfrac{1}{\phi^2}\left(\nabla\phi\cdot\overline{\mathbf{u}}^{\gamma}\right)\overline{\mathbf{u}}^{n+\theta_1} + Ra\,Pr\,\overline{T}_l^{n} \\ \\ \dfrac{\overline{T}_l^{n+1}-\overline{T}_l^{n}}{\Delta t} + \overline{\mathbf{u}}_l^{n+\theta_1}\cdot\nabla\overline{T}_l^{n+\theta_2} = \nabla\cdot\left(R_k\,\nabla\overline{T}_l^{n+\theta_2}\right) + R_h\left(1-\overline{T}_l^{n+\theta_2}\right) \end{cases} \tag{4}$$

Where:

$$\begin{aligned} \psi^{n+\theta_i} &= \theta_i\psi^{n+1} - (1-\theta_i)\psi^{n} \\ \psi^{\gamma} &= \psi^{n} + \gamma(\psi^{n} - \psi^{n-1}) \end{aligned} \tag{5}$$

In this algorithm, the momentum equation becomes linear for each time step with $\gamma \in [0,1]$ with an error proportional to Δt^2 for $\theta_1 = 0.5$ and $\gamma = 0.5$. While, for the energy equation, the algorithm becomes linear, unconditionally stable and with an error proportional to Δt^2 for $\theta_2 = 0.5$.

Another restriction becomes clear if we split the advective term of the momentum equation into:

$$\nabla\cdot\left(\frac{1}{\phi}\,\overline{\mathbf{u}}\,\overline{\mathbf{u}}\right) = \frac{\overline{\mathbf{u}}}{\phi}\nabla\overline{\mathbf{u}} - \frac{1}{\phi^2}(\nabla\phi\cdot\overline{\mathbf{u}})\overline{\mathbf{u}} \tag{6}$$

The first term on the right hand side takes the classic form of the advective operator of incompressible Navier-Stokes, while the second one is only relevant at the porous-free region transition. Here we denote the need for a continuous function for ϕ in our domain. In order to verify this condition, we use a sinusoidal function for ϕ at the transition.

3 RESULTS AND DISCUSSION

3.1 Code validation: clear square cavity problem

We studied the numerical solutions of a standard two-dimensional laminar natural convection problem to validate the code. The problem consists of a square cavity with fixed temperature on the lateral walls with $Pr = 0.71$ (see Figure 2). In Table 1, we present the mean Nusselt number at the lateral wall for $Ra = 10^8$, 10^9 and 10^{10} compared with results of Henkes et al. (1991) and Barakos et al. (1994). The agreement was excellent with an error lower than 3%.

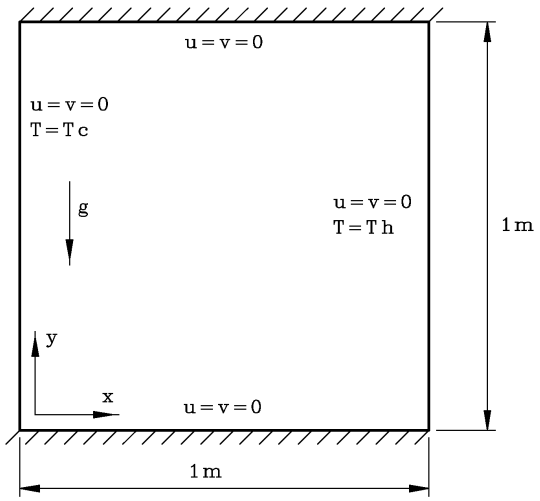

Figure 2: Schematic of the free square cavity problem

	$Ra = 10^8$	$Ra = 10^9$	$Ra = 10^{10}$
This work	29.7	52.9	96.5
Barakos $et\ al.$	30.1	54.4	97.6
Henkes $et\ al.$	30.4	54.1	-

Table 1: Steady state Nusselt number for the test case

3.2 Microscopic results

Our macroscopic problem is characterized by several dimensionless numbers ϕ, Pr, Ra, R_k and R_h. While at microscopic level, our problem simplifies as $\phi = 1$, $R_k = 1$ and $R_h = 0$. The Pr number was selected to maintain the properties of real fluids, so we use $Pr = 286$ which corresponds to a typical refrigerant oil of a power transformer. All in all, the problem is exclusively characterized by the Ra number.

One of the main goals of this work is to maintain similarities with real cases. In order to do this, we considered three aspects. The first one was already mentioned and it is related to the Pr number. The second one is based on having dimensions of the same order of magnitude of real engineering devices. Finally, we seek to have boundary conditions appropriated for real devices under operation. The last one becomes a critical issue with laminar simulations in which instabilities may arise. In this work, we adopted $Ra = 10^{10}$ as an upper limit (where we expect to obtain quasi-steady simulations) of the laminar regime. The three studied cases are:

1. $T_w = 293K, T_{obs} = 293.01K \Longrightarrow Ra = 1.4 \times 10^8$
2. $T_w = 293K, T_{obs} = 293.1K \Longrightarrow Ra = 1.4 \times 10^9$
3. $T_w = 293K, T_{obs} = 291K \Longrightarrow Ra = 1.4 \times 10^{10}$

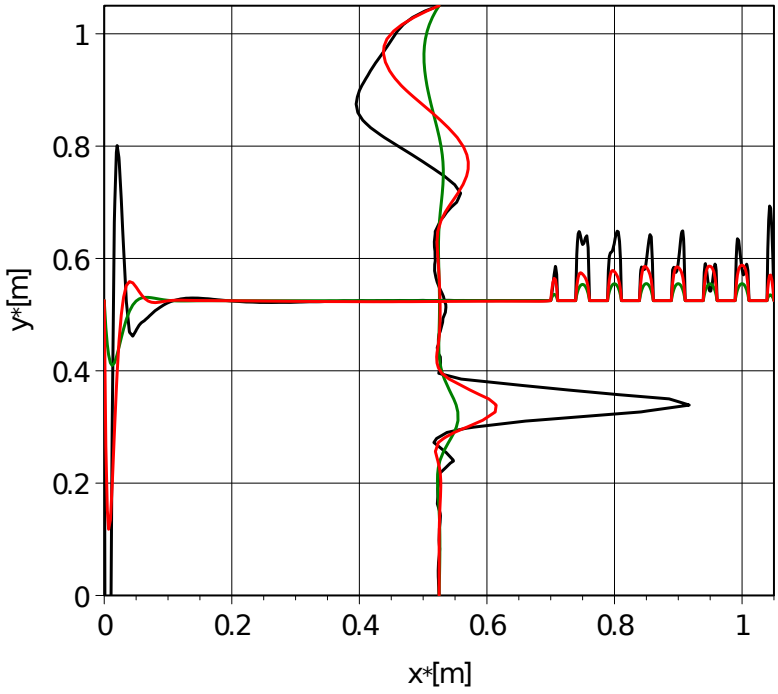

Figure 3: Horizontal and vertical centered dimensionless velocity profiles for $Ra = 10^8$ (green), $Ra = 10^9$ (red) and $Ra = 10^{10}$ (black)

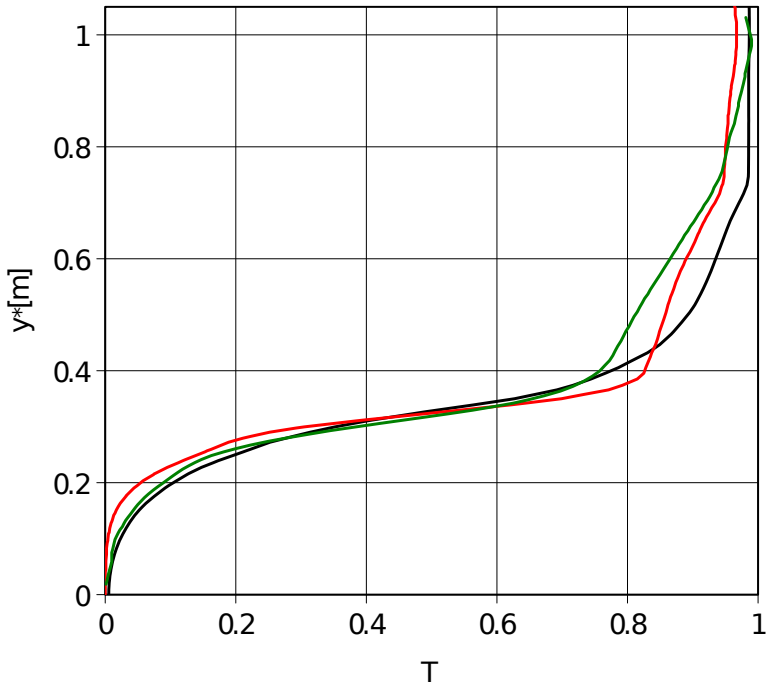

Figure 4: Dimensionless temperature profile at $x = 0.525$ m for $Ra = 10^8$ (green), $Ra = 10^9$ (red) and $Ra = 10^{10}$ (black)

The steady state horizontal velocity profile in a vertical centered plane at $x^* = 0.525$ m, and vertical velocity profile in a horizontal centered plane at $y^* = 0.525$ m are shown simultaneously in Figure 3. In every case, the flow is driven by buoyancy forces through the array of obstacles, then the flow circulates in the upper region of the cavity to the cold wall, and goes down at high velocity and lowering its temperature. Finally, the cycle completes with an inlet flow through the bottom of the obstacles region.

In Figure 4, the dimensionless temperature profiles at $x^* = 0.525$ m are shown. Here we can appreciate the same level of temperature stratification at $y^* \sim 0.35$ m.

In Table 2, we present the volumetric flow through the obstacles region and a measure of the energy transfer through a global Nusselt number. This global Nusselt number will be a function of the mean convective coefficient H and we will define it as follows:

$$Nu = \frac{HL}{k} = \int_0^L \left(\frac{1}{T_{obs} - T_w}\right)\left(\frac{\partial T^*}{\partial x^*}\right)_{x^*=0} dy^* \tag{7}$$

Case	Ra	Nu	$Q\ [\frac{cm^3}{s}]$
1	$\sim 10^8$	48.2	4.8
2	$\sim 10^9$	87.3	10.6
3	$\sim 10^{10}$	160.0	19.1

Table 2: Steady state Nusselt number for the microscopic model

For $Ra = 10^{10}$ we denoted fluctuations and a transient behavior of the velocity field. This point may be considered as the turbulence onset where numerical instabilities may growth due to the predominance of the buoyant term in the momentum equation.

3.3 Evaluation of macroscopic parameters

Based on the study of Dybbs and Edwards (1984) and the microscopic simulation results, we decided to neglect all inertial effects of the Darcy-Forchheimer theory (Ergun, 1952) for our model. This simplified formulation (1), is acceptable for problems with low Re number at the obstacles region ($Re \sim 1$).

The macroscopic problem, as it was previously discussed, is characterized by several dimensionless parameters. One of those is the porosity ϕ. We will define the porosity as the fraction of fluid volume to total volume (area for a two-dimensional problem) in a representative elementary volume (REV, see Figure 5). For an "in-line" array of circular obstacles we have:

$$\phi = \frac{dA_l}{dA} = 1 - \pi\left(\frac{r}{L}\right)^2 = 0.75 \tag{8}$$

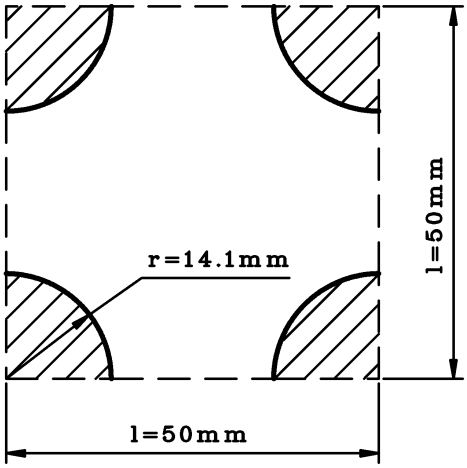

Figure 5: Representative elementary volume for an "in-line" arrangement

The Carman-Kozeny equation is a well known correlation to calculate the permeability coefficient for structures as those modeled in this study (see Kaviany (1995)). This equation is based on forced flow experiments, and was implemented by several authors (Massarotti et al., 2003; Braga and de Lemos M.J., 2005). In this work, we found that the use of the Darcy model (where the permeability and the Da number is related only to the geometry of the REV) may not be suitable for natural convection problems. This is due to an apparent relationship between the flow resistance and the Ra number. Based on this, we decided to use the Darcy model with a modified Da number. The criteria was to adjust the Da number to maintain the same volumetric flow through the porous media for each Ra number. With this modification, the geometry of the obstacles cease to be the only factor that influences the Da number.

For the R_k calculation, we used the experimental correlation obtained by Eidsath et al. (1983) for an in-line array of circular obstacles:

$$\frac{k_e}{k} = 1 + 0.7Pe^{1.2} \quad (\text{for } \; Pe \geq 1) \tag{9}$$

Where:

$$Pe = \frac{D\phi|\overline{\mathbf{u}}|}{1.5\alpha(1-\phi)} \quad (\text{for } \; \phi \leq 0.9) \tag{10}$$

For the calculation of R_h we use the results of the microscopic simulation and a solution proposal for the one-dimensional macroscopic energy balance equation on a vertical line at the porous region:

$$R_h = \frac{R_k}{L^2}T_m^2 - \frac{|\overline{\mathbf{u}}|}{L}T_m \tag{11}$$

Where:

$$T_m = ln\frac{(T_{out} - T_{obs})}{(T_{in} - T_{obs})} \tag{12}$$

In Table 3 we summarize the macroscopic parameters that characterize this problem for each Ra number:

Parameter	Free region	Porous region		
		$Ra = 10^8$	$Ra = 10^9$	$Ra = 10^{10}$
ϕ	1	0.75	0.75	0.75
$Da\ (\times 10^{-6})$	∞	33.0	16.3	2.6
R_k	1.34	36.15	75.02	149.90
R_h	0	9146.7	10453.3	32666.7

Table 3: Summary of the macroscopic parameters

3.4 Macroscopic results and comparison

In Figures 6, 7 and 8, we present a qualitative comparison between models for the dimensionless velocity profiles for $Ra = 10^8$, $Ra = 10^9$ and $Ra = 10^{10}$ respectively.

In Figures 9, 10 and 11, the stratification level may be appreciated comparing the thermal profiles for both models at $x = 0.525$ m.

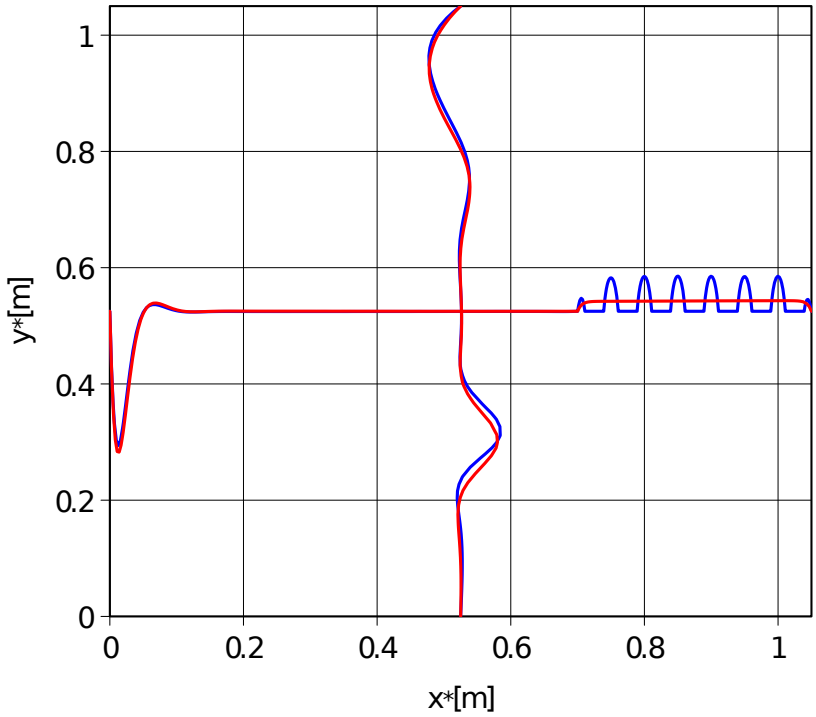

Figure 6: Velocity profiles with the microscopic model (blue) and the macroscopic model (red) for $Ra = 10^8$

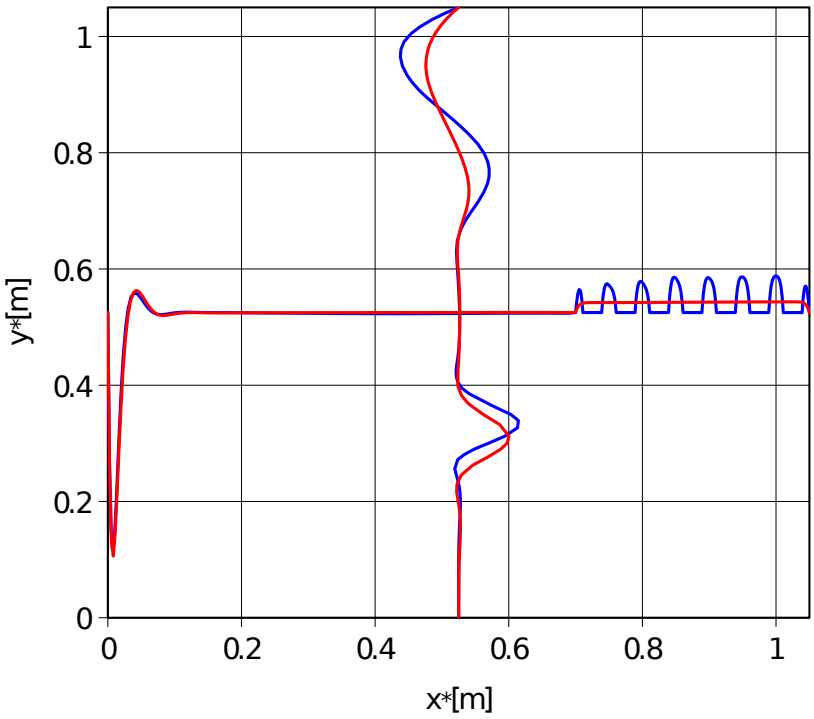

Figure 7: Velocity profiles with the microscopic model (blue) and the macroscopic model (red) for $Ra = 10^9$

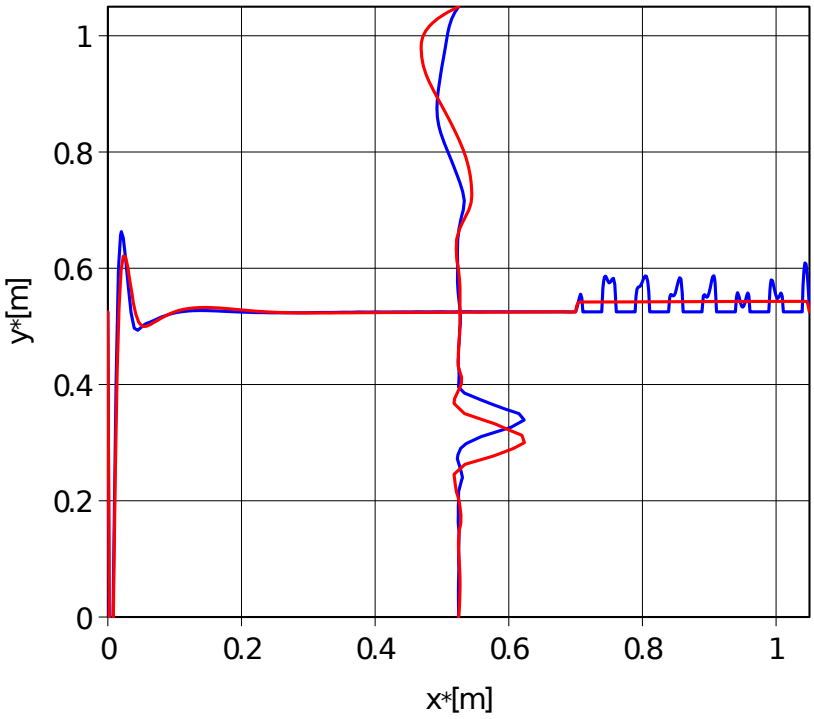

Figure 8: Velocity profiles with the microscopic model (blue) and the macroscopic model (red) for $Ra = 10^{10}$

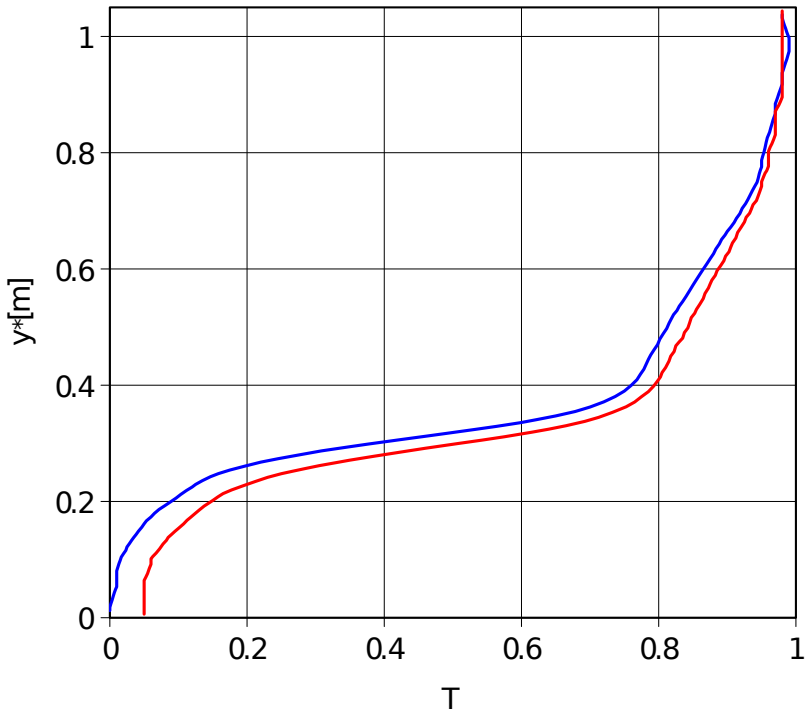

Figure 9: Temperature profiles with the microscopic model (blue) and the macroscopic model (red) for $Ra = 10^8$

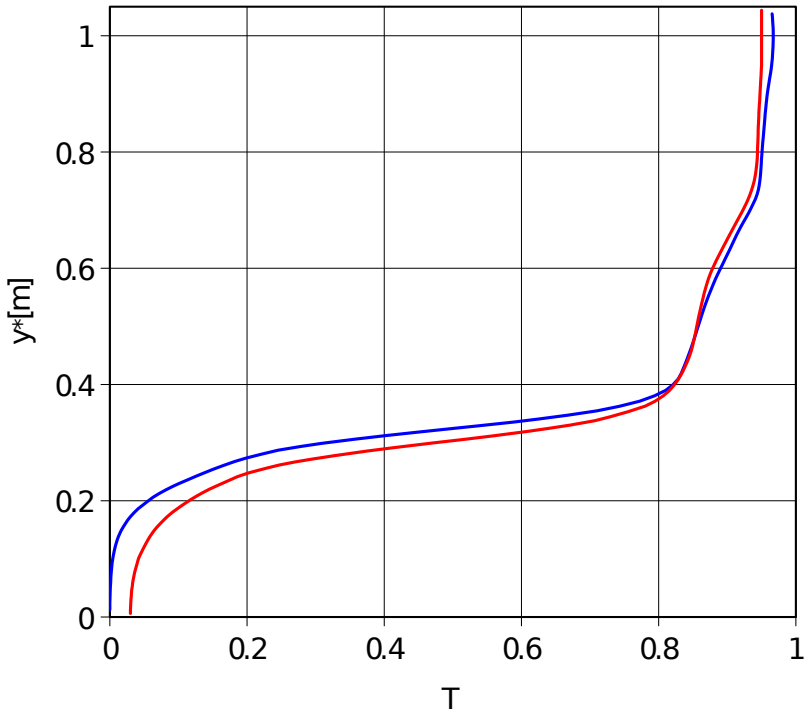

Figure 10: Temperature profiles with the microscopic model (blue) and the macroscopic model (red) for $Ra = 10^9$

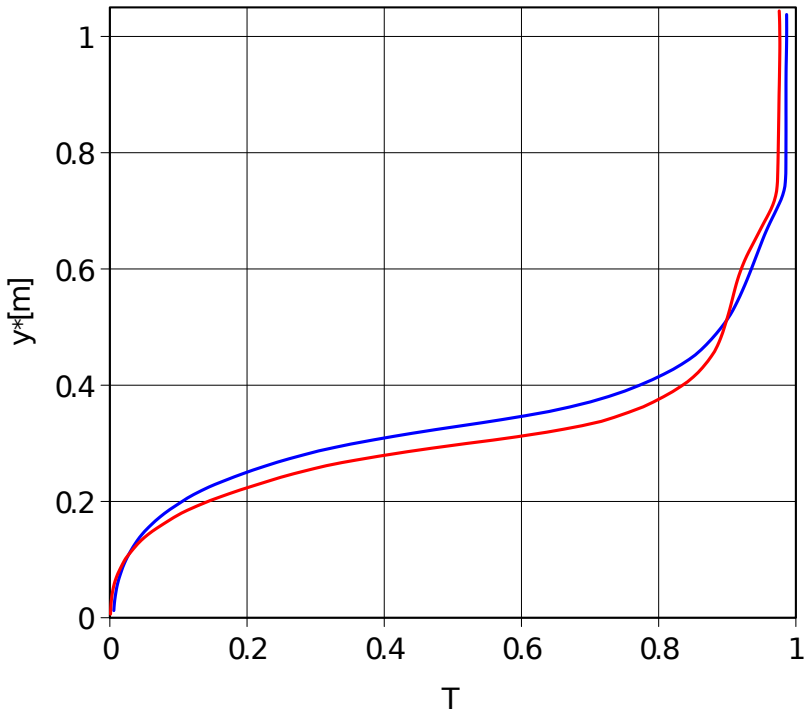

Figure 11: Temperature profiles with the microscopic model (blue) and the macroscopic model (red) for $Ra = 10^{10}$

In Table 4 we present a comparison of the energy transfer for $Ra = 10^9$ (i.e. the mean Nusselt number) at the cold wall for both models. The largest difference between both models is lower than 5% for the range of Ra number simulated. Figures 12, shows the energy transfer on a local level to point out that, for each position on the cold wall, the same amount of energy is transferred with both models.

Ra	Microscopic model	Macroscopic model
10^8	48.2	50.7
10^9	87.3	88.8
10^{10}	160.0	163.3

Table 4: Mean Nusselt number for each case

An important remark is that, for the macroscopic simulations, we were able to successfully implement the model and carry out simulations in a third of the computational time spent for the microscopic model.

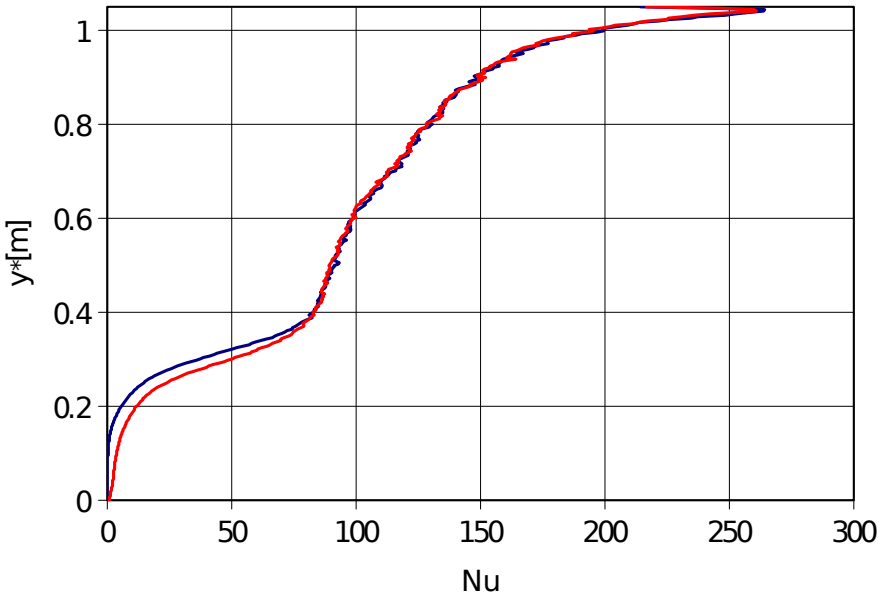

Figure 12: Local Nusselt number at the cold wall with the microscopic model (blue) and the macroscopic model (red) for $Ra = 10^9$

4 CONCLUSIONS

In this work we have been able to numerically implement a macroscopic model on a FEM-based program, that simulates both thermal and dynamical behavior of a flow in a natural convection regime circulating through an obstructed media. In order to do this, we use physical models to represent the effects of the obstacles on the fluid. These models use a set of macroscopic parameters that need to be calculated. One approach to obtain these parameters (that has been used by many authors) is to use correlations based on forced flow experiments. We have seen that this approach may not be correct for flow dominated by natural convection and we may conclude that a proper study for a natural convection regime may be needed to develop accurate models. In order to maintain similarities with real cases, we selected real fluid properties, real dimensions and real boundary conditions when possible (due the flow become unstable for large temperature gradients). The performance of the macroscopic model was accurate in both levels: qualitative and quantitative. We found similarities in the dynamical behavior of the flow and stratification levels. We also found the same behavior in both the mean and local heat transfer coefficient. Although there is still dependence on the microscopic model to calculate the macroscopic parameters, the computational cost of a macroscopic simulation was lowered to a third of that spent for the microscopic model. This means that, with the development of the proper natural convection porous media models, the use of a macroscopic approach could become a strong low-cost tool to solve industrial scale problems.

NOTATION

A_{LS}	interphase surface, m^2
dA	averaging region surface, m^2
dV	averaging region volume, m^3
D	obstacles diameter, m
Da	Darcy number
g	gravity acceleration, m/s^2
H	global convective coefficient, $W/m^2.K$
k	thermal conductivity, W/m.K
k_e	equivalent thermal conductivity, W/m.K
K	permeability, m^2
l	REV characteristic lenght, m
L	square cavity lenght, m
n	time step index
Nu	global Nusselt number
p	pressure, Pa
Pe	Peclet number
Pr	Prandtl number
Q	volumetric flow, cm^3/s
r	obstacles radius, m
Ra	Rayleigh number
Re	Reynolds number
R_h	macroscopic convective coefficient
R_k	macroscopic conductivity coefficient
u	velocity, m/s
t	time, s
T	temperature, K
T_0	reference temperature, K
T_m	logarithmic mean temperature, K
T_{obs}	obstacles temperature, K
T_w	wall temperature, K
ΔT	temperature difference between obstacles and cold wall, K
x	horizontal lenght/lenght scale, m
y	vertical lenght, m
α	thermal diffusivity, m^2/s
β	thermal expansion coefficient, 1/K
γ	gamma coefficient
θ	theta coefficient
ν	kinematic viscosity, m^2/s
ρ	density, Kg/m^3
ρ_0	reference density, Kg/m^3
ϕ	porosity
ψ	generic scalar
$\boldsymbol{\psi}$	generic tensor (of order > 1)
$\overline{\psi}$	volume averaged variable
$\overline{\psi}_l$	liquid-volume averaged variable
ψ^*	dimensioned variable

REFERENCES

Babuska I. Error-bounds for finite element method. *Numerische Mathematik*, 16:322–333, 1971.

Barakos G., Mitsoulis E., and Assimacopoulos D. Natural convection flow in a square cavity revisited: Laminar and turbulent models with wall functions. *International Journal for Numerical Methods in Fluids*, 18:695–719, 1994.

Braga E. and de Lemos M.J. Heat transfer in enclosures having a fixed amount of solid material simulated with heterogeneous and homogeneous models. *International Journal of Heat and Mass Transfer*, 48:4748–4765, 2005.

Brezzi F. On the existence, uniqueness and approximation of saddle-point problems arising from lagrangian multipliers. *R.A.I.R.O. Analyse Numerique*, 8:129–151, 1974.

Brinkman H. A calculation of the viscous force exerted by a flowing fluid on a dense swarm of particles. *Applied Scientific Research*, 1:28–34, 1947.

Buscaglia G. *GPFEP, Un sistema de generacion de programas de elementos finitos*, 1995.

Carbonell R. and Whitaker S. Heat and mass transfer in porous media. *Fundamentals of Transport Phenomena in Porous Media*, 82:121–198, 1984.

Codina R. and Blasco J. Stabilized finite element method for transient navier-stokes equations based on a pressure gradient projection. *Computer Methods in Applied Mechanical and Engineering*, 182:277–300, 2000.

Dybbs A. and Edwards R. A new look at porous media fluid mechanics - darcy to turbulent. *Fundamentals of Transport Phenomena in Porous Media*, 82:199–254, 1984.

Eidsath A., Carbonell R., Whitaker S., and Herrmann L. Dispersion in pulsed systems-iii comparison between theory and experiments for packed beds. *Chemical Engineering Science*, 38:1803–1816, 1983.

Ergun S. Fluid dlow through packed columns. 48:89–94, 1952.

Hassanizadeh M. and Gray W. General conservation equations for multi-phase systems: 1.averaging procedure. *Advances in Water Resources*, 2:131–144, 1979a.

Hassanizadeh M. and Gray W. General conservation equations for multi-phase systems: 2.mass, momenta, energy and entropy equations. *Advances in Water Resources*, 2:191–203, 1979b.

Henkes R., Vlugt R., and Hoogendoorn C. Natural convection flow in a square cavity calculated with low-reynolds-number turbulence models. *International Journal of Heat and Mass Transfer*, 34:1543–1557, 1991.

Kaviany M. *Principles of heat transfer in porous media*. Springer, 1995.

Massarotti N., Nithiarasu P., and Carotenuto A. Microscopic and macroscopic approach for natural convection in enclosures filled with fluid saturated porous medium. *International Journal of Numerical Methods for Heat and Fluid Flow*, 13:862–886, 2003.

Merrikh A. and Lage J. Natural convection in an enclosure with disconnected and conducting solid blocks. *International Journal of Heat and Mass Transfer*, 48:1361–1372, 2005.

Slattery J. Single-phase flow through porous media. *AIChE J.*, 15:866–872, 1969.

Whitaker S. Advances in theory of fluid motion in porous media. *Indutrial and Engineering Chemistry*, 61:14–28, 1969.

Whitaker S. The forchheimer equation: A theoretical development. *Transport in Porous Media*, 25:27–61, 1996.